

See discussions, stats, and author profiles for this publication at: <https://www.researchgate.net/publication/237044131>

Theoretical Modeling of Leading Edge Vortices Using the Leading Edge Suction Parameter

Conference Paper · June 2012

DOI: 10.2514/6.2012-3027

CITATIONS

10

READS

1,120

5 authors, including:



Kiran Ramesh
Arizona State University
47 PUBLICATIONS 828 CITATIONS

[SEE PROFILE](#)



Ashok Gopalarathnam
North Carolina State University
132 PUBLICATIONS 2,077 CITATIONS

[SEE PROFILE](#)



Michael Ol
121 PUBLICATIONS 3,383 CITATIONS

[SEE PROFILE](#)

Journal version of this article (also available for download):

“Discrete-vortex method with novel shedding criterion for unsteady airfoil flows with intermittent leading-edge vortex shedding,” *Journal of Fluid Mechanics*, 751:500-538.

Theoretical Modeling of Leading Edge Vortices Using the Leading Edge Suction Parameter

Kiran Ramesh,* Ashok Gopalarathnam†

*Department of Mechanical and Aerospace Engineering,
North Carolina State University, Raleigh, NC 27695-7910*

Kenneth Granlund,‡ Michael V. Ol,§

*U.S. Air Force Research Laboratory, Air Vehicles Directorate,
AFRL/RBAA, Bldg. 45, 2130 8th St., WPAFB, OH 45433-7542*

Jack R. Edwards,¶

*Department of Mechanical and Aerospace Engineering,
North Carolina State University, Raleigh, NC 27695-7910*

A theoretical low-order model to predict the forces and flow evolution on airfoils and flat plates undergoing arbitrary 2D unsteady maneuvers is presented. An inviscid airfoil theory with discrete vortex shedding from the trailing edge is augmented with a Leading Edge Suction Parameter (LESP), which is a criterion to predict leading edge separation. The LESP is used to mediate intermittent discrete vortex shedding from the leading edge. This model is validated against CFD and experiment for motions in recent unsteady airfoil literature. In addition, the influences of leading and trailing edge vortices on the force histories are studied in detail by examining the various constituents of forces on the airfoil from theory. Overall, the model is seen to be successful in predicting forces and flow evolution for unsteady motions.

Nomenclature

α	angle of attack
$\dot{\alpha}$	pitch rate
h	plunge rate
$\eta(x)$	variation of camber along airfoil
$\gamma(x, t)$	chordwise vorticity distribution
$\gamma_m(x)$	bound vorticity due to airfoil motion
Γ_{b_t}	bound circulation of airfoil at time t
$\gamma_{lev}(x)$	bound vorticity due to leading edge vortices
$\gamma_{tev}(x)$	bound vorticity due to trailing edge vortices
Γ_{lev_n}	strength of n^{th} leading edge vortex
Γ_{tev_m}	strength of m^{th} trailing edge vortex
ω	frequency of sinusoidal motion
ϕ_B	velocity potential from bound circulation
ϕ_{lev}	velocity potential from leading edge vortices
ϕ_l	lower surface velocity potential

*Graduate Research Assistant, Box 7910, kramesh2@ncsu.edu, (919) 600-0519. Student Member, AIAA

†Associate Professor, Box 7910, ashok_g@ncsu.edu, (919) 515-5669. Associate Fellow, AIAA

‡Post-Doctoral Scholar, kenneth.granlund@WPAFB.AF.MIL, Member,AIAA

§Aerospace Engineer, Michael.Ol@WPAFB.AF.MIL, Associate Fellow, AIAA

¶Professor, Box 7910, jredward@ncsu.edu, (919) 515-5264. Associate Fellow, AIAA

ϕ_{tev}	velocity potential from trailing edge vortices
ϕ_u	upper surface velocity potential
ρ	fluid density
θ	variable of transformation of chordwise distance
a	pivot location on the airfoil from 0 to 1 (x/c)
A_0, A_1, A_2, \dots	Fourier coefficients
B_{xyz}	body frame
c	airfoil chord
C_d	drag coefficient
C_l	lift coefficient
C_m	pitching moment coefficient
C_N	normal force coefficient
C_S	leading edge suction force coefficient
cm_{pvt}	pivot for pitching moment calculation
h	plunge displacement
K	reduced frequency, $\frac{\dot{a}c}{2U}$
k	reduced frequency for sinusoidal motion, $\frac{\omega c}{2U}$
M	moment on airfoil
N	normal force on airfoil
$OXYZ$	inertial frame
$p(x)$	pressure on airfoil surface
t	time
t^*	non-dimensional time, $\frac{tU}{c}$
U	freestream velocity
V_t	tangential velocity on airfoil surface
$W(x, t)$	local downwash
x	chordwise distance
LESP	leading edge suction parameter

I. Introduction

Unsteady flow phenomena occur in a wide range of problems in current aerospace engineering research. These include, but are not limited to: rotorcraft dynamic stall, delta-wing aerodynamics, wind-power devices, insect flight modeling and micro air vehicle (MAV) design. This paper builds on previous work by the authors in low Reynolds number unsteady aerodynamics pertaining to insect flight and MAVs. Some aspects of MAVs which influence aerodynamic considerations are their necessarily small sizes, low speeds and low Reynolds numbers. Insects employ flapping flight with high dimensionless rates of motion to achieve remarkable flying prowess in these very regimes. Hence it has become clear that understanding and emulating the aerodynamic phenomena involved in insect flight would aid the design of highly maneuverable and agile MAVs.

The single most important aerodynamic phenomenon largely responsible for the success of flapping flight at low Reynolds numbers has been identified as the Leading Edge Vortex (LEV).^{1–4} LEV formation is initiated by separation at the airfoil leading edge. This separation bubble builds up into a vortex, which traverses the airfoil chord and convects into the wake, causing large deviation in all force coefficients (lift, drag and moment) from attached flow behavior. High-lift flight in insects, such as that seen during hovering is accomplished largely owing to the effects of LEVs.

Classical unsteady theories, the most prominent of which are the methods of Theodorsen⁵ and Wagner,⁶ have been employed successfully in aeroelasticity. However, these have limited application in the problems under consideration since they do not account for LEVs, and use assumptions of small amplitudes and planar wakes. A new theoretical model accounting for large amplitudes of motion and nonplanar wakes was developed by the authors⁷ and applied to a pitch up-hold-pitch down maneuver. The results from the theoretical model were compared against those from computational (immersed boundary) and experimental (water tunnel) methods. The theoretical model was seen to be successful except in LEV dominated regions of flow. Hence it was apparent that a working method to predict the onset and phenomenologically model the effect of LEVs is required. Advances in CFD and experiment have enabled the detailed study of LEV phenomena.^{8–11} A computational method to predict the formation of LEVs has been developed by Jones *et*

al.¹² However, for use in design and real-time simulation, a low-order theoretical method is needed.

Dynamic stall encountered in helicopters has prompted the rotorcraft community to develop methods for studying the onset and effects of LEVs.^{13,14} A number of semi-empirical methods to model dynamic stall have been developed for use in rotor analysis and design. A brief description of these models, along with a demonstration of their capabilities is given in Ref. 15. These rely on empirical parameters and can only be used in conditions bounded by validation with experimental data. Some low order unsteady airfoil theories, such as those given in Refs. 16 and 17, model the effects of leading edge vortices on the flowfield and forces. These methods, however, assume separation at the leading edge and do not define conditions where it is initiated. In previous work by the authors,¹⁸ a Leading Edge Suction Parameter (LESP) was developed, the critical value of which corresponds to separation initiated at the leading edge. In the current paper, the LESP is used in conjunction with a discrete vortex method to predict and model LEVs in highly unsteady flows.

II. Theoretical Formulation

Sarkpaya,¹⁹ Katz²⁰ and other researchers have developed discrete vortex models for separated flows with commendable success. The current research proposes to extend our Large Angle Unsteady Thin Airfoil Theory⁷ along similar lines, while employing the LESP criterion¹⁸ to supersede *ad hoc* conjectures of when the flow is attached or separated at the leading edge.

II.A. Time stepping approach

Details of this time stepping method can be found in Refs. 7 and 21. The inertial frame is given by $OXYZ$ and the body frame attached to the airfoil is given by $Bxyz$. At time $t = 0$, the body frame is assumed to coincide with the inertial frame and at time $t > 0$, moves towards the left of the page along a prescribed path. At each discrete time-step, a trailing-edge vortex is shed from the trailing-edge as shown in Figure 1. Leading edge vortices are shed in accordance with the LESP criterion which will be elaborated on in Section II.C.

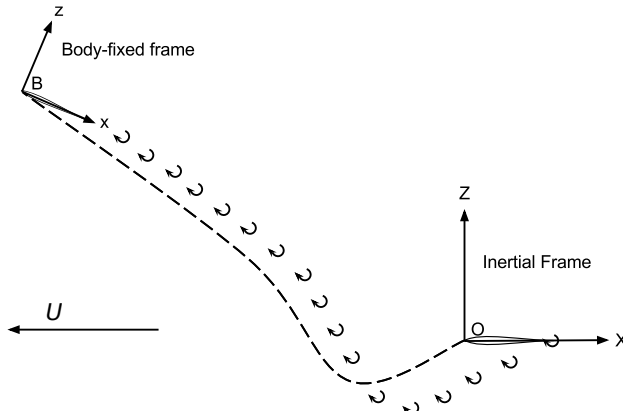


Figure 1. An illustration of the time stepping method.

The vorticity distribution over the airfoil is taken to be a Fourier series in a manner analogous to thin-airfoil theory,

$$\gamma(\theta, t) = 2U(t) \left[A_0(t) \frac{1 + \cos \theta}{\sin \theta} + \sum_{n=1}^{\infty} A_n(t) \sin(n\theta) \right] \quad (1)$$

where,

$$x = \frac{1}{2}(1 - \cos \theta) \quad (2)$$

θ varies from 0 to π as x varies from 0 to 1 along the airfoil.

II.B. Calculation of local downwash and Fourier coefficients

The Fourier coefficients are given in terms of the local downwash $W(x, t)$ as:

$$A_0(t) = -\frac{1}{\pi} \int_0^\pi \frac{W(x, t)}{U(t)} d\theta \quad (3)$$

$$A_n(t) = \frac{2}{\pi} \int_0^\pi \frac{W(x, t)}{U(t)} \cos n\theta d\theta \quad (4)$$

The local downwash is calculated by enforcing the boundary condition of zero normal flow on the airfoil surface.

$$W(x, t) \equiv \frac{\partial \phi_B}{\partial z} = \frac{\partial \eta}{\partial x} (U \cos \alpha + h \sin \alpha + \frac{\partial \phi_{lev}}{\partial x} + \frac{\partial \phi_{tev}}{\partial x}) - U \sin \alpha - \dot{\alpha}(x - ac) + h \cos \alpha - \frac{\partial \phi_{tev}}{\partial z} - \frac{\partial \phi_{lev}}{\partial z} \quad (5)$$

where $\frac{\partial \phi_{lev}}{\partial x}$ and $\frac{\partial \phi_{tev}}{\partial x}$ are velocities induced along the chord by leading and trailing edge discrete vortices and $\frac{\partial \phi_{lev}}{\partial z}$ and $\frac{\partial \phi_{tev}}{\partial z}$ are the induced velocities normal to the chord. The calculation of these quantities is detailed in section II.D.

The unknown at each time step is the strength of the last shed trailing edge vortex, assuming that no leading edge vortex is formed at this time step. This is calculated iteratively using a Newton-Raphson iteration to satisfy Kelvin's condition.

$$\Gamma_{b_t} + \sum_{m=1}^{n_{tev}} \Gamma_{tev_m} + \sum_{n=1}^{n_{lev}} \Gamma_{lev_n} = 0 \quad (6)$$

where Γ_{b_t} is the bound circulation calculated by integrating the chordwise vorticity over the airfoil chord:

$$\Gamma_{b_t} = U(t)c\pi \left[A_0(t) + \frac{A_1(t)}{2} \right] \quad (7)$$

II.C. LESP criterion and condition for LEV shedding

The Leading Edge Suction Parameter (LESP) is a measure of the suction peak at the leading edge, which in turn is caused by the stagnation point moving away from the leading edge to some other location when the airfoil is at an angle of attack. As the airfoil thickness approaches zero, the leading edge radius also approaches zero, giving rise to a theoretically infinite velocity at the leading edge. The suction peak which determines the limit of attached flow at the leading edge, is calculated as a function of this velocity.

From Refs. 22 and 23, we have that the true magnitude of the theoretically infinite velocity can be found as:

$$V_{LE}(t) = \frac{1}{\sqrt{2}} \lim_{x \rightarrow LE} \gamma(x, t) \sqrt{x} \quad (8)$$

The Leading Edge Suction Parameter is defined as the quantity obtained by nondimensionalizing the leading edge velocity by the instantaneous freestream velocity. Evaluating using the current formulation gives:

$$LESP(t) = A_0(t) \quad (9)$$

In previous work,¹⁸ it was demonstrated that for a given airfoil and Reynolds number, there is a critical value of the LESP which determines whether or not the flow is attached at the leading edge, irrespective of motion kinematics. The positive value of LESP determines the limit of attached flow for the airfoil's upper surface and negative value for the lower surface. The flow is said to be separated when the LESP exceeds the critical value and reattached when the LESP goes below the critical value.

The critical value of LESP for a given airfoil and Reynolds number needs to be obtained using existing experimental or computational results with the same airfoil and Reynolds number. The LESP from theory, corresponding to the instant of separation in any unsteady motion is the critical value. Using this, LEV phenomena can be predicted for any desired motion kinematics. An example of quantitatively calculating the $LESP_{crit}$ from CFD is shown in Figure 2. A pitch up-hold-pitch down motion with pivot about the trailing edge, reduced frequency of 0.2 and at a Reynolds number of 1000 is considered for this example.

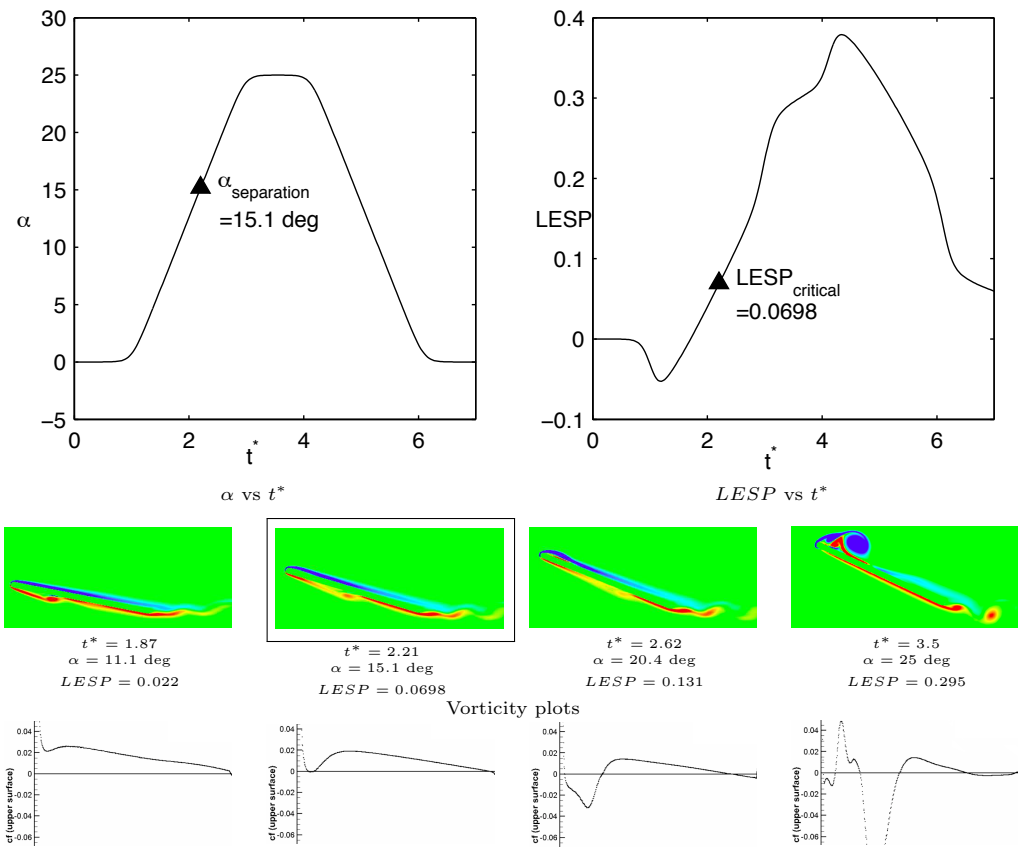


Figure 2. Example of LESP calibration using CFD

The instant at which the skin friction coefficient from CFD becomes negative near the leading edge is taken to indicate the onset of leading edge separation. The LESP value from theory at this instant is the critical LESP for a flat plate at $Re = 1000$.

Hence in the current model, if the LESP at a time step ($A_0(t)$) exceeds the critical value, a leading edge vortex is shed. The strength of the leading edge vortex is determined by iteration to satisfy the requirement that the value of the LESP is brought back to $LESP_{critical}$. This models the expected behavior that rounded leading edges support a certain amount of suction even when flow at the leading edge is separated.²⁰

II.D. Vortex method details

Discrete vortex models usually involve positioning the last shed vortex along the path of the shedding edge (eg. Katz [20]). In the current model, the placement methodology given by Ansari *et al.*^{16,24} is used, where the latest vortex is placed at one-third of the distance from the shedding edge to the previous shed vortex. This method takes into account both the airfoil motion and the convection of the previous shed vortex, thereby describing the flow more accurately.

$$(x, z)_{tev_i/lev_i} = (x, z)_{TE/LE} + \frac{1}{3}((x, z)_{tev_{i-1}/lev_{i-1}} - (x, z)_{TE/LE}) \quad (10)$$

The position of first shed vortex at the leading edge is calculated as a function of the velocity at the leading edge. Note that trailing edge vortices are shed at every time step but leading edge vortices are shed only when the LESP is in excess of the critical value. Hence the position of the first shed vortex is calculated only once (at the start of motion) for TEVs but may be calculated on more than one occasion for LEVs (each time the formation of a new LEV sheet is initiated). In this model, the first vortices are placed as follows:

$$(x, z)_{tev_1} = (x, z)_{TE} + \frac{1}{2}(U, 0)\delta t \quad (11)$$

$$(x, z)_{lev_1} = (x, z)_{LE} + \frac{1}{\sqrt{2}}(UA_0 \sin \alpha, UA_0 \cos \alpha)\delta t \quad (12)$$

Traditionally, the Biot-Savart law is used to calculate the velocities induced by point vortices at other points in the field. However, using a singular vortex model leads to very high induced velocities when the distance between vortices is small. Here, the vortex model proposed by Vatistas *et al.*²⁵ is used, which gives a very good approximation to the Lamb-Oseen vortex. Using Vatistas vortex model with order 2, we have that the velocities induced by the k^{th} vortex in the X and Z directions (u and w) are :

$$u = \frac{\gamma_k}{2\pi} \frac{z - z_k}{\sqrt{((x - x_k)^2 + (z - z_k)^2)^2 + v_{core}^4}} \quad (13)$$

$$w = -\frac{\gamma_k}{2\pi} \frac{x - x_k}{\sqrt{((x - x_k)^2 + (z - z_k)^2)^2 + v_{core}^4}} \quad (14)$$

Vortices that cross through the airfoil during convection, are reflected back. It was seen that this methodology was more robust than deleting the vortices, which led to large oscillations in the solution.

II.E. Pressure distribution, forces and moment on airfoil

From the unsteady Bernoullis equation, we have:

$$\Delta p(x) = p_l(x) - p_u(x) \quad (15)$$

$$= \rho \left(\frac{1}{2}(V_{t_u}^2 - V_{t_l}^2) + \left(\frac{\partial \phi}{\partial t} \right)_u - \left(\frac{\partial \phi}{\partial t} \right)_l \right) \quad (16)$$

$$\phi = \phi_b + \phi_{lev} + \phi_{tev} \quad (17)$$

$$V_{t_u} = U \cos \alpha + h \sin \alpha + \left(\frac{\partial \phi_{lev}}{\partial x} \right)_u + \left(\frac{\partial \phi_{tev}}{\partial x} \right)_u + \left(\frac{\partial \phi_b}{\partial x} \right)_u \quad (18)$$

$$V_{t_l} = U \cos \alpha + h \sin \alpha + \left(\frac{\partial \phi_{lev}}{\partial x} \right)_l + \left(\frac{\partial \phi_{tev}}{\partial x} \right)_l + \left(\frac{\partial \phi_b}{\partial x} \right)_l \quad (19)$$

$$(20)$$

Drawing from thin airfoil theory:

$$\left(\frac{\partial \phi_b}{\partial x} \right)_u = \frac{\gamma(x)}{2} \quad (21)$$

$$\left(\frac{\partial \phi_b}{\partial x} \right)_l = -\frac{\gamma(x)}{2} \quad (22)$$

$$V_{t_u}^2 - V_{t_l}^2 = 2 \left(U \cos \alpha + \dot{h} \sin \alpha + \left(\frac{\partial \phi_{lev}}{\partial x} \right) + \left(\frac{\partial \phi_{tev}}{\partial x} \right) \right) \gamma(x) \quad (23)$$

$$\phi_u = \int_0^x \frac{\gamma(x)}{2} dx + \int_0^x \left(\frac{\partial \phi_{lev}}{\partial x} \right) dx + \int_0^x \left(\frac{\partial \phi_{tev}}{\partial x} \right) dx \quad (24)$$

$$\phi_l = - \int_0^x \frac{\gamma(x)}{2} dx + \int_0^x \left(\frac{\partial \phi_{lev}}{\partial x} \right) dx + \int_0^x \left(\frac{\partial \phi_{tev}}{\partial x} \right) dx \quad (25)$$

$$\left(\frac{\partial \phi}{\partial t} \right)_u - \left(\frac{\partial \phi}{\partial t} \right)_l = \frac{\partial}{\partial t} \int_0^x \gamma(x) dx \quad (26)$$

From equations 16, 23 and 26,

$$\Delta p(x) = \rho \left(U \cos \alpha + \dot{h} \sin \alpha + \left(\frac{\partial \phi_{lev}}{\partial x} \right) + \left(\frac{\partial \phi_{tev}}{\partial x} \right) \right) \gamma(x) + \frac{\partial}{\partial t} \int_0^x \gamma(x) dx \quad (27)$$

The first term is similar to the steady state circulatory term and the second includes the contribution of time dependency/fluid acceleration. Following the terminology used in Katz and Plotkin,²¹ the first term is called the circulatory contribution and the second term is called the apparent mass.

With the aim of analyzing the contributions of different phenomena towards the normal force as described above, we split the bound vorticity into components stemming from airfoil motion, leading edge vortices and trailing edge vortices:

$$\gamma(x) = \gamma_m(x) + \gamma_{lev}(x) + \gamma_{tev}(x) \quad (28)$$

The Fourier coefficients for the different bound vorticity components (motion, lev, tev) may be obtained by integrating the specific components of local downwash on the airfoil (eqns: 3 and 5).

The normal force on the airfoil is obtained by integrating the pressure distribution over the airfoil chord.

$$N = \int_0^c \Delta p(x) dx \quad (29)$$

$$C_N = \frac{N}{\frac{1}{2} \rho U^2 c} \quad (30)$$

We split the normal force into the following four components:

- $C_{N_{C,m}}$ - Circulatory component caused by motion.
- $C_{N_{C,w}}$ - Circulatory components caused by wake vortices (both LEVs and TEVs).
- $C_{N_{AM,m}}$ - Apparent mass component caused by motion.
- $C_{N_{AM,w}}$ - Apparent mass component caused by wake vortices.

$$C_{N_{C,m}} = \frac{2}{U^2 c} (U \cos \alpha + h \sin \alpha) \int_0^c \gamma_m(x) dx \quad (31)$$

$$= 2\pi \left(\cos \alpha + \frac{h}{U} \sin \alpha \right) \left(A_{0m} + \frac{A_{1m}}{2} \right) \quad (32)$$

$$\begin{aligned} C_{N_{C,w}} &= \frac{2}{U^2 c} \left(\int_0^c \left(\left(\frac{\partial \phi_{tev}}{\partial x} \right)_x + \left(\frac{\partial \phi_{lev}}{\partial x} \right)_x \right) (\gamma_m(x) + \gamma_{tev}(x) + \gamma_{lev}(x)) dx \right) \\ &\quad + \frac{2}{U^2 c} \left((U \cos \alpha + h \sin \alpha) \int_0^c (\gamma_{tev}(x) + \gamma_{lev}(x)) dx \right) \end{aligned} \quad (33)$$

$$\begin{aligned} &= \frac{2}{U^2 c} \int_0^c \left(\left(\frac{\partial \phi_{tev}}{\partial x} \right)_x + \left(\frac{\partial \phi_{lev}}{\partial x} \right)_x \right) (\gamma_m(x) + \gamma_{tev}(x) + \gamma_{lev}(x)) dx \\ &\quad + 2\pi \left(\cos \alpha + \frac{h}{U} \sin \alpha \right) \left(A_{0_{tev}} + A_{0_{lev}} + \frac{A_{1_{tev}}}{2} + \frac{A_{1_{lev}}}{2} \right) \end{aligned} \quad (34)$$

The first term in the circulatory wake component is evaluated numerically. Details on the derivation of the second term in terms of Fourier coefficients, can be found in Refs. 7 and 21.

$$C_{N_{AM,m}} = \frac{2}{U^2 c} \int_0^c \frac{\partial}{\partial t} \int_0^x \gamma_m(x) dx \quad (35)$$

$$= 2\pi \frac{c}{U} \left(\frac{3}{4} \dot{A}_{0m} + \frac{1}{4} \dot{A}_{1m} + \frac{1}{8} \dot{A}_{2m} \right) \quad (36)$$

$$C_{N_{AM,w}} = 2\pi \frac{c}{U} \left(\frac{3}{4} (\dot{A}_{0_{tev}} + \dot{A}_{0_{lev}}) + \frac{1}{4} (\dot{A}_{1_{tev}} + \dot{A}_{1_{lev}}) + \frac{1}{8} (\dot{A}_{2_{tev}} + \dot{A}_{2_{lev}}) \right) \quad (37)$$

In addition to the normal force, there is a leading edge suction force acting axial to the airfoil, given by the Blasius formula:

$$C_S = \pi \rho b V_{LE}^2 \quad (38)$$

Employing the current formulation gives:

$$C_S = 2\pi A_0^2 \quad (39)$$

The lift and drag forces on the airfoil are comprised of components from the normal and leading edge suction forces:

$$C_l = C_N \cos \alpha + C_S \sin \alpha \quad (40)$$

$$C_d = C_N \sin \alpha - C_S \cos \alpha \quad (41)$$

The pitching moment coefficient of the airfoil, about a pivot cm_{pvt} is given by:

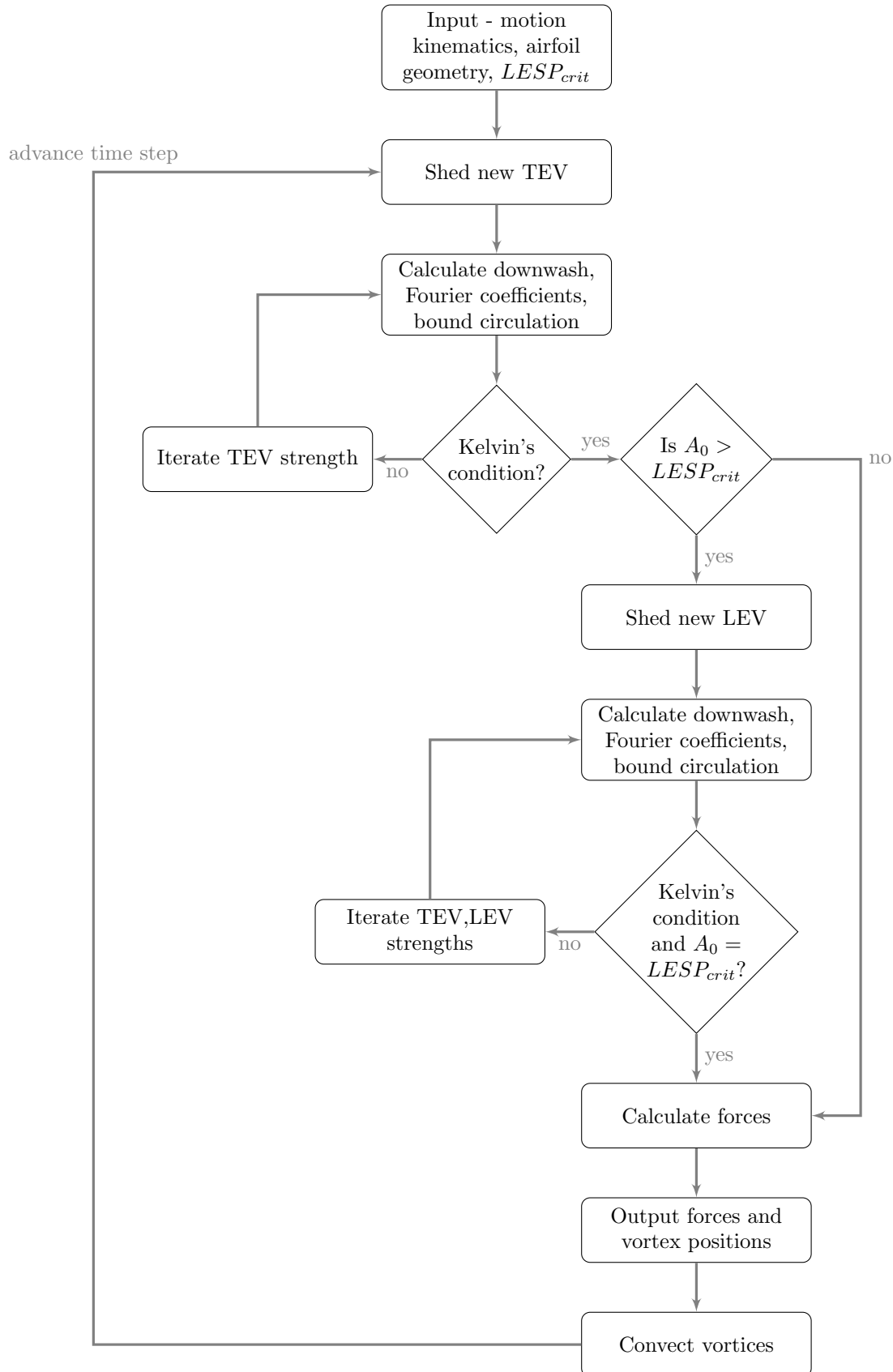
$$M = \int_0^c \Delta p(x)(x - cm_{pvt}) dx \quad (42)$$

$$C_m = \frac{M}{\frac{1}{2} \rho U^2 c^2} \quad (43)$$

II.F. Convection of vortices

All leading edge and trailing edge vortices are convected with the local velocity at their positions, at each time step. The local velocity at the vortex locations includes contributions from bound, leading edge and trailing edge vortices. Details on calculating the induced velocity due to vortices are given in section II.D.

II.G. Summary of model - Flowchart



III. Results and Discussion

The theoretical model developed in section II is validated against results from experiment and/or computation. Motions kinematics employed in recent studies of unsteady flows^{8,9,26,27} and of interest to the low Reynolds number community, are used for validation, and the various constituents of forces on the airfoil as derived in section II.E are examined.

III.A. Pitch up-hold-pitch down maneuvers

Previous studies of pitch up-hold-pitch down motions of a flat plate by the authors⁷ revealed that LEVs were responsible for large deviations in force coefficients from inviscid theoretical predictions. These motions are now used to validate the current theoretical model against experiment (performed at AFRL's Horizontal Free-surface Water Tunnel^{11,28,29}) and computation (immersed boundary method^{7,30,31}). Two pitch-hold maneuvers of amplitudes 25 and 45 deg, with pivot about the leading edge are considered. These motions have reduced frequencies of $K = 0.11$ rad and $K = 0.2$ rad respectively and the Reynolds number of operation is 10,000. The $LESP_{crit}$ for a flat plate at $Re = 10,000$ has been pre-calibrated from CFD to be 0.02. This single value of $LESP_{crit}$ is the only parameter introduced in the theoretical calculation from either experiment or CFD.

III.A.1. 25 deg pitch-hold

Figures 3 and 4 show comparisons of lift coefficient and drag coefficient respectively. The points A, B, C and D marked in the figures are used for analyzing the flow history, later in this section.

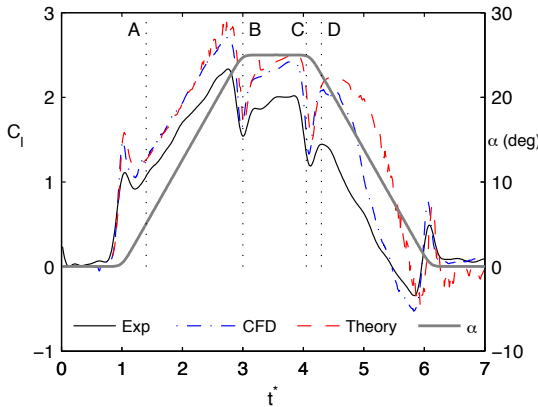


Figure 3. 25-deg pitch about leading edge: Comparison of C_l from experiment, CFD and theory.

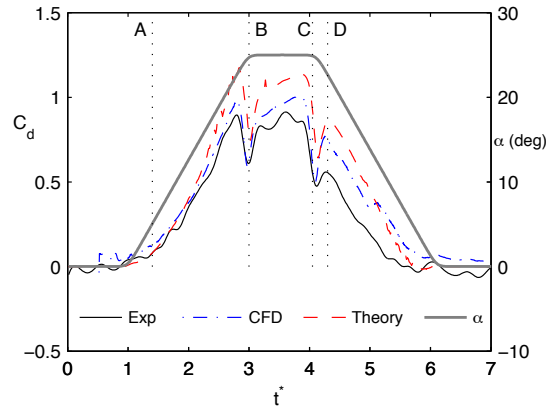


Figure 4. 25-deg pitch about leading edge: Comparison of C_d from experiment, CFD and theory.

A good match in lift coefficient between CFD and theory is seen, with the C_l from experiment begin a little lower than the predictions from CFD and theory. In an effort to analyze the contributions of various phenomena towards the forces, the components of normal force as derived in section II.E are plotted in Figure 5. The pitching moment and $LESP$ histories calculated from theory are shown in Figure 6. The pitching moment for this case is calculated about the airfoil leading edge.

To compare flow evolution from different methods, discrete vortex plots from theory are compared against vorticity contours from CFD and dye-flow visualization from experiment at the four time instants A, B, C and D.

The point A corresponds to the start of LEV formation. Points B and C show the flow visualization at the start and end of the hold respectively. The point D corresponds to detachment of the LEV when it reaches the trailing edge, subsequently resulting in flow reversal over the surface of the airfoil. Good agreement in the flow visualization, is seen between experiment, CFD and theory at all four time instants.

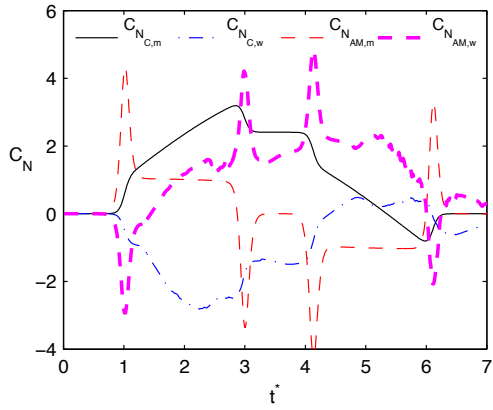


Figure 5. 25-deg pitch about leading edge: Components C_N from theory.

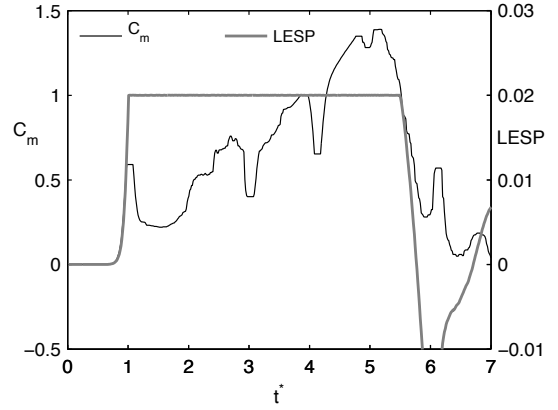


Figure 6. 25-deg pitch about leading edge: C_m and LESP from theory.

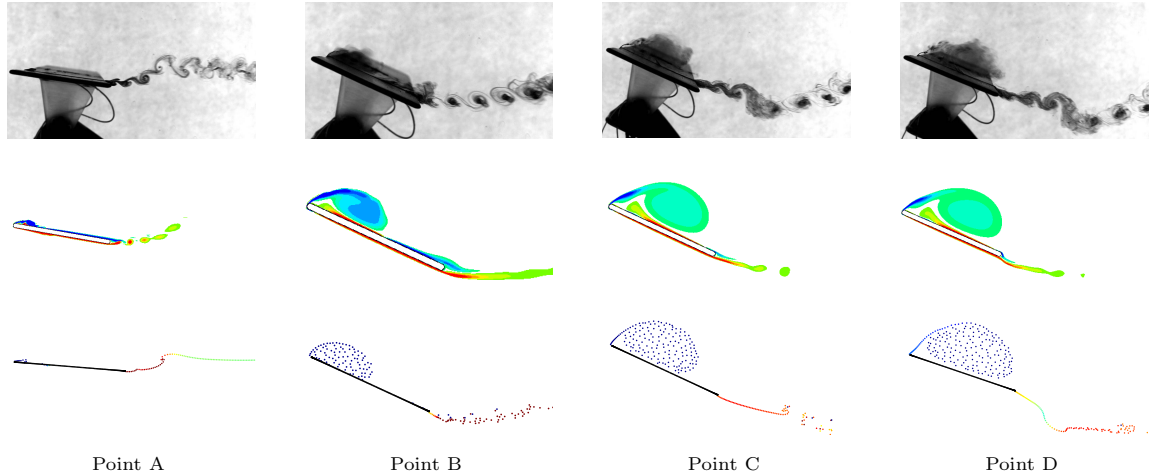


Figure 7. 25-deg pitch about leading edge: Flow visualization from experiment (top), CFD (middle) and theory (bottom).

III.A.2. 45 deg pitch-hold

Comparisons of lift and drag coefficients are shown in Figures 8 and 9 respectively.

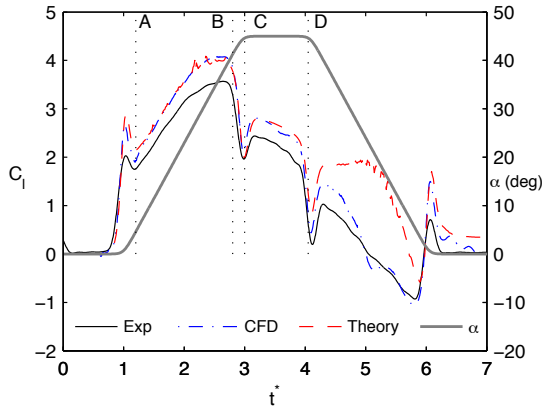


Figure 8. 45-deg pitch about leading edge: Comparison of C_l from experiment, CFD and theory.

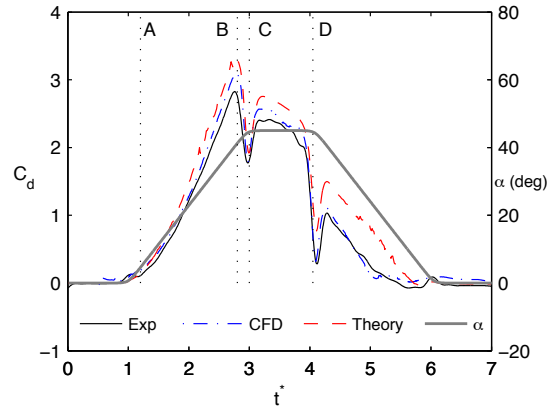


Figure 9. 45-deg pitch about leading edge: Comparison of C_d from experiment, CFD and theory.

The components of normal force for this case are shown in Figure 10 and the C_m and LESP histories in Figure 11.

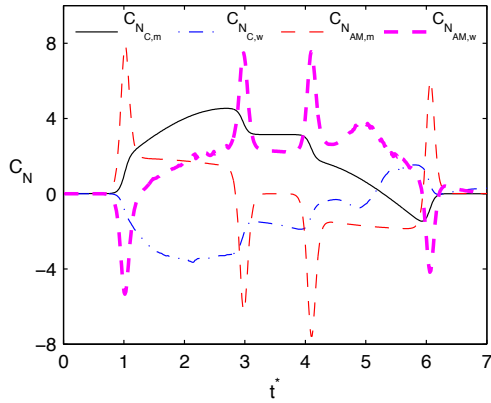


Figure 10. 45-deg pitch about leading edge: Components of C_N from theory.

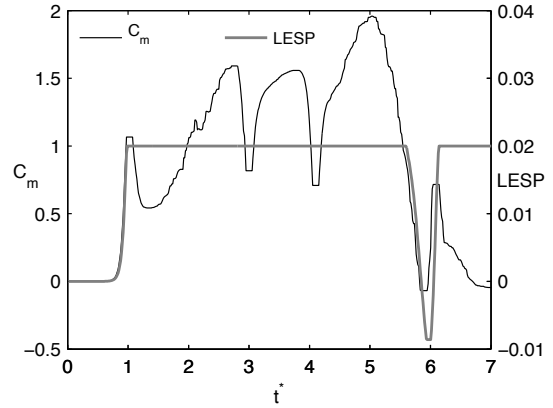


Figure 11. 45-deg pitch about leading edge: C_m and LESP from theory.

Comparisons of flow evolution from experiment, CFD and theory at the time instants given in Figure 8 and 9 are shown in Figure 12.

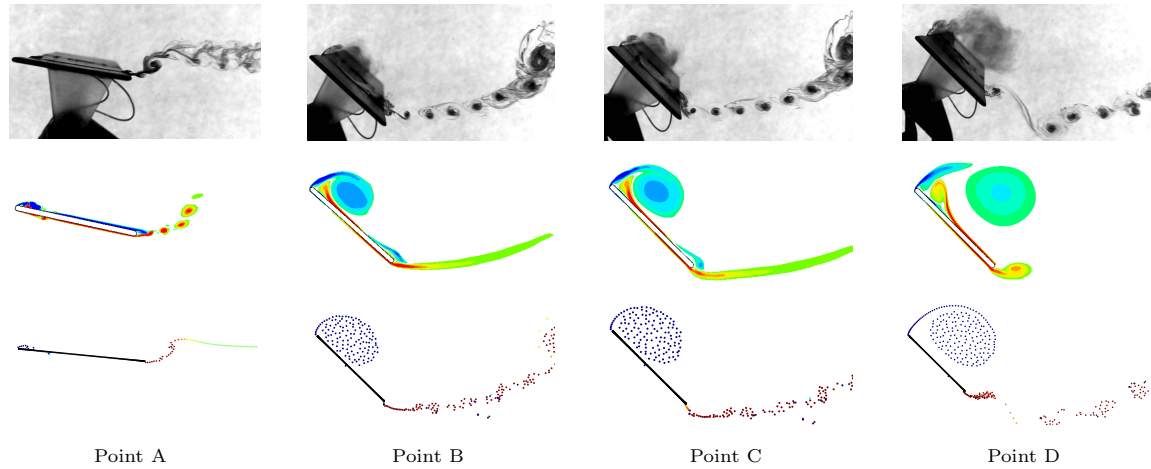


Figure 12. 45-deg pitch about leading edge: Flow visualization from experiment (top), CFD (middle) and theory (bottom).

Point A again denotes the start of LEV formation. Point B corresponds to the detachment of the vortex (lift-off from airfoil surface), which occurs at the end of the upstroke in this case. C and D show the flow visualization at the beginning and end of the hold. Good agreement in forces and flow evolution is seen between experiment, CFD and theory.

The LESP history from Figure 11 shows the LESP reaching the critical value after the end of the motion. This suggests that the LEV and TEV effects cause the flow to get separated at the leading edge even after the motion has ended. The dye-flow visualization from experiment, at a time after the end of the downstroke, confirms that this does indeed happen.



Figure 13. Flow separated at the leading edge after end of motion from experiment (left) and theory (right).

III.B. 90 deg Pitch-ramp motion

A 90 deg pitch-ramp of a flat plate at $Re = 1000$, with $K = 0.2$ and pivot about the leading edge is analyzed in this section. Results from theory are validated against results from a viscous vortex particle simulation (couplevpm code) by Wang and Eldredge.^{32,33} The $LESP_{crit}$ for a flat plate at $Re = 1000$ was pre-determined from CFD (immersed boundary method⁷) to be 0.07.

Comparisons of lift and drag coefficient are given in Figures 14 and 15. The four time instants used for flow comparison A, B, C and D are marked. These are located at equally spaced intervals in the motion.

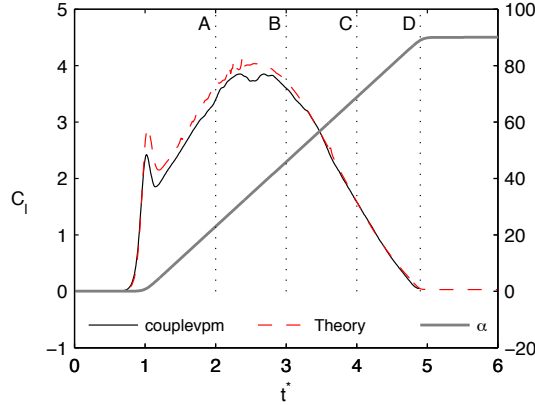


Figure 14. 90-deg pitch-ramp: Comparison of C_l .

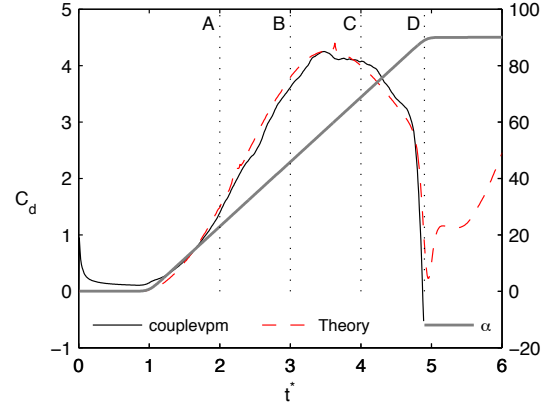


Figure 15. 90-deg pitch-ramp: Comparison of C_d .

The circulatory and apparent mass constituent components of normal force are given in Figure 16. Comparison of C_m histories from the two methods about the half-chord is shown in Figure 17. The reason for the C_m from theory not matching too well with C_m from the couplevpm code is not clear.

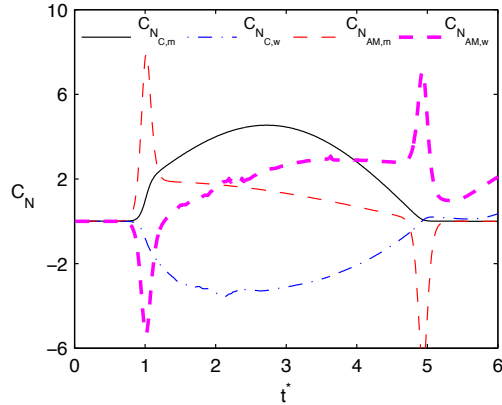


Figure 16. 90-deg pitch-ramp: Components of C_N from theory.

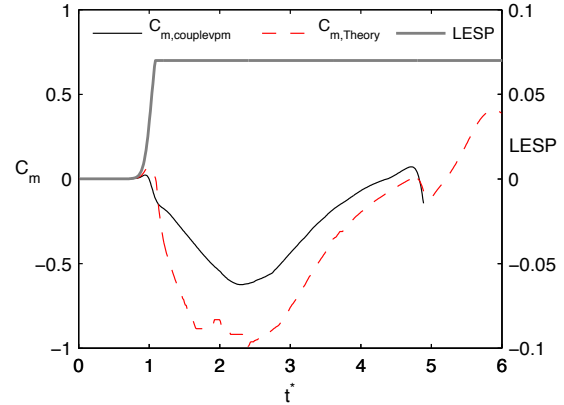


Figure 17. 90-deg pitch-ramp: Comparison of C_m and LESP history from theory.

The discrete vortex plots from theory are compared against those from the couplevpm simulation at the time instants A, B, C and D (Figure 18).

An excellent agreement in flow evolution and force histories from the two methods is seen.

III.C. Sinusoidal plunge

In this section, an SD7003 airfoil undergoing a pure plunge oscillation ($h_{amp} = 0.05$) with a mean angle of attack of 4° , reduced frequency of $k = 3.93$ and at a Reynolds number of 10,000 is considered. This case is chosen from the set of sinusoidal pitch-plunge combination cases analyzed in Refs. 34 and 26. Experiments were performed at the U.S. AFRL horizontal free-surface water tunnel and computational results were

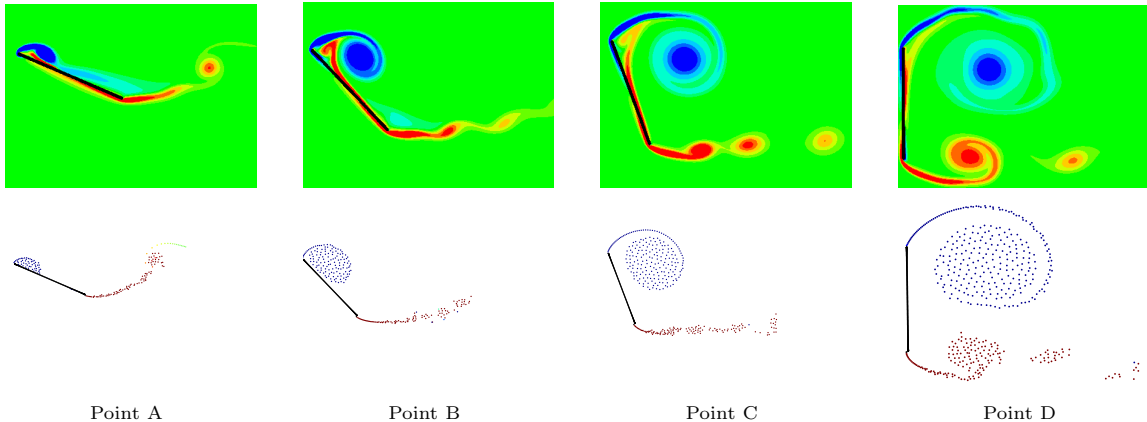


Figure 18. 90 deg pitch-ramp about leading edge: Flow visualization from high-fidelity simulation (top) and theory (bottom).

obtained using the CFL3D code. The $LESP_{crit}$ for an SD7003 airfoil at $Re = 10,000$, was determined from experimental dye-flow visualization to be 0.18.

Comparisons of lift and drag from experiment, CFD and theory are shown in Figures 19 and 20.

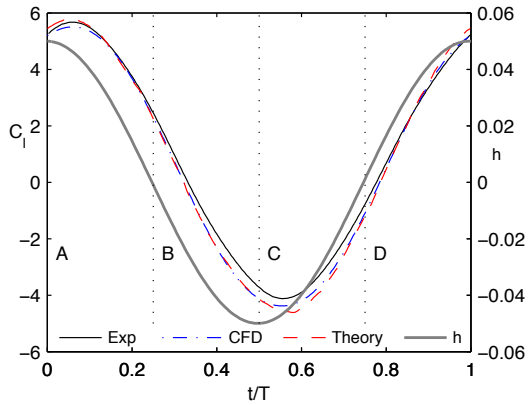


Figure 19. Sinusoidal plunge: Comparison of C_l .

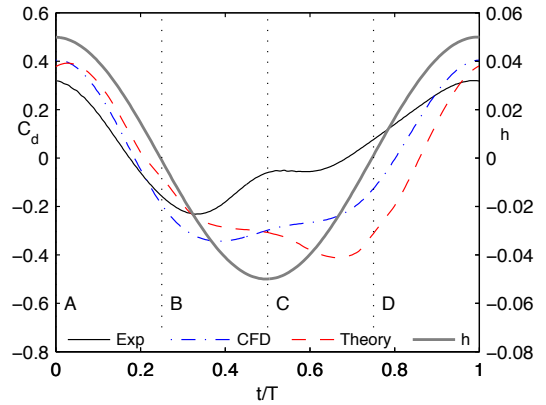


Figure 20. Sinusoidal plunge: Comparison of C_d .

Again, the circulatory and apparent mass contributions to the normal force are plotted in Figure 21. Pitching moment histories, derived from experiment, CFD and theory (about the quarter chord) are compared in Figure 22. The $LESP$ history from theory is also plotted in this figure.

The discrete vortex flow from theory is compared against dye-flow from experiment at the points A, B, C, and D in Figure 23.

Again, the theory is seen to predict well in terms of both flow evolution and force histories. It is worth noting that this case exhibits multiple LEVs - At point C in the flow, there are two LEVs on the airfoil upper surface and one on the lower surface. All these phenomena are successfully captured and replicated by the $LESP$ -mediated discrete vortex shedding approach developed in this effort.

IV. Summary

In this paper, a discrete vortex method to predict forces and flow evolution for arbitrary unsteady motions is presented. The $LESP$ criterion,¹⁸ used to modulate the discrete vortex shedding, is integrated with the unsteady inviscid airfoil theory previously developed by the authors⁷ to model leading edge vortex phenomena. It was attempted to phenomenologically augment inviscid theory (using discrete vortices and the $LESP$ criterion) to model the viscous events occurring in unsteady flows. On validation with a number of motions seen in recent literature of unsteady flows, the model was seen to be successful.

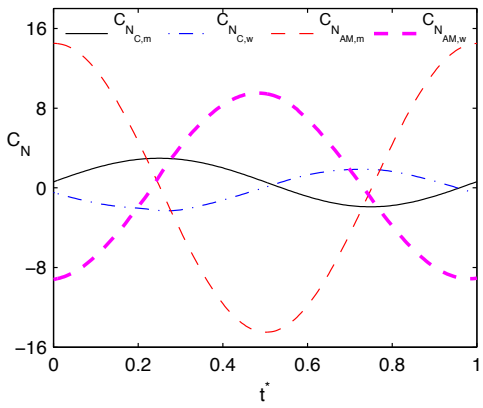


Figure 21. Sinusoidal plunge: Components of C_N from theory.

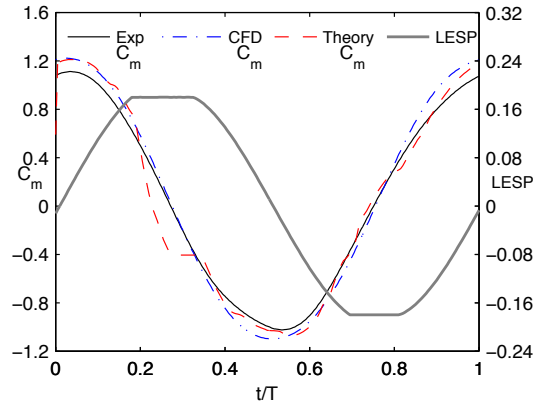


Figure 22. Sinusoidal plunge: Comparison of C_m and LESP history.

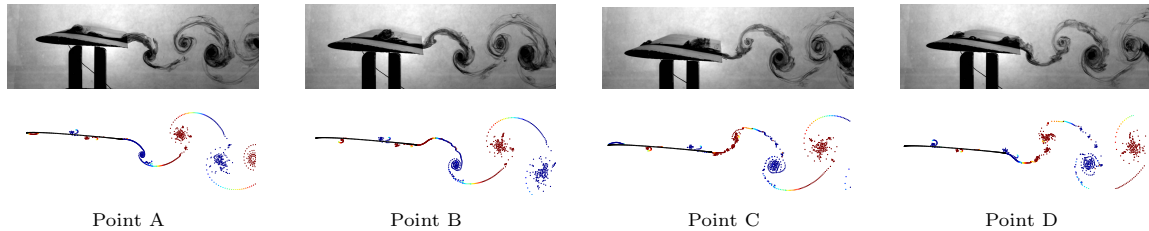


Figure 23. Sinusoidal plunge: Flow visualization from experiment (top) and theory (bottom).

Future work includes augmentation of the current model to account for trailing edge separation as well. In flows such as those examined in this paper, the effect of LEVs and apparent mass forces overshadow trailing edge separation. However, in motions with lower reduced frequencies and higher Reynolds number (such as those of interest to the rotorcraft community), modeling of trailing edge separation becomes necessary. The model will also be extended to handle varying freestream velocities so that perching and hovering maneuvers may be examined using theory. Though this low-order method is fast (typical run times < 1 min), it could be made faster with the use of multipole methods^{35,36} to handle the discrete vortices or vortex amalgamation methods.³⁷ These will be studied to build a faster low-order model for unsteady flows.

V. Acknowledgments

The authors wish to gratefully acknowledge the support of the U.S. Air Force Office of Scientific Research through grant FA 9550-10-1-0120; program manager: Douglas Smith.

References

- ¹Ellington, C., Van Den Berg, C., Willmott, A., and Thomas, A., "Leading-edge vortices in insect flight," *Nature*, Vol. 384, 1996, pp. 626–630.
- ²Shyy, W. and Liu, H., "Flapping Wings and Aerodynamic Lift: The Role of Leading-Edge Vortices," *AIAA journal*, Vol. 45, No. 12, 2007.
- ³Ellington, C., "The novel aerodynamics of insect flight: applications to micro-air vehicles," *Journal of Experimental Biology*, Vol. 202, No. 23, 1999, pp. 3439–3448.
- ⁴Dickinson, M. and Gotz, K., "Unsteady aerodynamic performance of model wings at low Reynolds numbers," *Journal of Experimental Biology*, Vol. 174, No. 1, 1993, pp. 45–64.
- ⁵Theodorsen, T., "General Theory of Aerodynamic Instability and the Mechanism of Flutter," NACA Rept. 496, 1935.
- ⁶Wagner, H., "Über die Entstehung des dynamischen Auftriebes von Tragflügeln," *ZaMM*, Vol. 5, No. 1, 1925, pp. 17–35.
- ⁷Ramesh, K., Gopalarathnam, A., Edwards, J. R., Granlund, K., and Ol, M. V., "Theoretical, computational and experimental studies of a flat plate undergoing high-amplitude pitching motion," AIAA Paper 2011-0217, 2011, Submitted to Journal of Theoretical and Computational Fluid Dynamics.
- ⁸Eldredge, J. D., Wang, C., and Ol, M. V., "A computational study of a canonical pitch-up, pitch-down wing maneuver."

AIAA paper 2009-3687, 2009.

⁹Eldredge, J. D. and Wang, C., "High-fidelity simulations and low-order modeling of a rapidly pitching plate." AIAA paper 2010-4281, 2010, In review for publication in *Journal of Theoretical and Computational Fluid Dynamics*.

¹⁰"Experiments and computations on abstractions of perching." Tech. rep.

¹¹Ol, M., Bernal, L., Kang, C., and Shyy, W., "Shallow and deep dynamic stall for flapping low Reynolds number airfoils," *Experiments in fluids*, Vol. 46, No. 5, 2009, pp. 883–901.

¹²Jones, K. and Platzer, M., "On the prediction of dynamic stall onset on airfoils in low speed flow," *Proceedings of the 8th International Symposium on Unsteady Aerodynamics and Aeroelasticity of Turbomachines*, 1998, pp. 797–812.

¹³McCroskey, W., "The phenomenon of dynamic stall." NASA TM-81264, 1981.

¹⁴Leishman, J. and Beddoes, T., "A Semi-Empirical Model for Dynamic Stall," *Journal of the American Helicopter Society*, Vol. 34, 1989, pp. 3–17.

¹⁵Leishman, J. G., *Principles of Helicopter Aerodynamics*, Cambridge Aerospace Series, Cambridge University Press, Cambridge, 2002.

¹⁶Ansari, S., Źbikowski, R., and Knowles, K., "Non-linear unsteady aerodynamic model for insect-like flapping wings in the hover. Part 1: methodology and analysis," *Proceedings of the Institution of Mechanical Engineers, Part G: Journal of Aerospace Engineering*, Vol. 220, No. 2, 2006, pp. 61–83.

¹⁷Eldredge, J. and Wang, C., "Improved low-order modeling of a pitching and perching plate," AIAA Paper 2011-3579, 2011.

¹⁸Ramesh, K., Gopalarathnam, A., Ol, M. V., Granlund, K., and Edwards, J. R., "Augmentation of Inviscid Airfoil Theory to Predict and Model 2D Unsteady Vortex Dominated Flows," AIAA Paper 2011-3578, 2011.

¹⁹Sarpkaya, T., "An inviscid model of two-dimensional vortex shedding for transient and asymptotically steady separated flow over an inclined plate," *Journal of Fluid Mechanics*, Vol. 68, No. 01, 1975, pp. 109–128.

²⁰Katz, J., "Discrete Vortex Method for the Non-Steady Separated Flow Over an Airfoil," *Journal of Fluid Mechanics*, Vol. 102, 1981, pp. 315–328.

²¹Katz, J. and Plotkin, A., *Low-Speed Aerodynamics*, Cambridge Aerospace Series, 2000.

²²Garrick, I., "Propulsion of a Flapping and Oscillating Airfoil," NACA Rept. 567, 1937.

²³von Kármán, T. and Burgers, J., *General Aerodynamic Theory - Perfect Fluids*, Vol. 2 of Aerodynamic theory: a general review of progress, Durand, W. F. , Dover Publications, 1963.

²⁴Ansari, S., Źbikowski, R., and Knowles, K., "Non-linear unsteady aerodynamic model for insect-like flapping wings in the hover. Part 2: implementation and validation," *Proceedings of the Institution of Mechanical Engineers, Part G: Journal of Aerospace Engineering*, Vol. 220, No. 3, 2006, pp. 169–186.

²⁵Vatistas, G., Kozel, V., and Mih, W., "A simpler model for concentrated vortices," *Experiments in Fluids*, Vol. 11, No. 1, 1991, pp. 73–76.

²⁶McGowan, G. Z., Granlund, K., Ol, M. V., Gopalarathnam, A., and Edwards, J. R., "Investigations of Lift-Based Pitch-Plunge Equivalence for Airfoils at Low Reynolds Numbers," *AIAA Journal*, Vol. 49, No. 7, July 2011, pp. 1511–1524.

²⁷Ol, M. V., Altman, A., Eldredge, J. D., Garmann, D. J., and Lian, Y., "Résumé of the AIAA FDTC Low Reynolds Number Discussion Group's Canonical Cases," AIAA Paper 2010-1085, January 2010.

²⁸Granlund, K., Ol, M. V., and Bernal, L., "Experiments on Pitching Plates : Force and Flowfield measurements at Low Reynolds Numbers," AIAA Paper 2011-0872, 2011.

²⁹Ol, M., McAuliffe, B., Hanff, E., Scholz, U., and Kaehler, C., "Comparison of laminar separation bubble measurements on a low Reynolds number airfoil in three facilities," AIAA Paper 2005-5149, 2005.

³⁰Cassidy, D. A., Edwards, J. R., and Tian, M., "An investigation of interface-sharpening schemes for multi-phase mixture flows," *Journal of Computational Physics*, Vol. 228, No. 16, 2009, pp. 5628 – 5649.

³¹Neaves, M. D. and Edwards, J. R., "All-Speed Time-Accurate Underwater Projectile Calculations Using a Preconditioning Algorithm," *Journal of Fluids Engineering*, Vol. 128, No. 2, 2006, pp. 284–296.

³²Eldredge, J., "Numerical simulation of the fluid dynamics of 2D rigid body motion with the vortex particle method," *Journal of Computational Physics*, Vol. 221, No. 2, 2007, pp. 626–648.

³³Wang, C. and Eldredge, J., "Low-order phenomenological modeling of leading-edge vortex formation," *submitted to Journal of Theoretical and Computational Fluid Dynamics*, 2012.

³⁴Granlund, K., McGowan, G. Z., Gopalarathnam, A., Ol, M. V., and Edwards, J. R., "The validity bounds of analytical force and moment predictions for pitch and plunge oscillating low Reynolds number airfoil," AIAA Paper 2010-8126, 2010.

³⁵Willis, D., Peraire, J., and White, J., "A combined pFFT-multipole tree code, unsteady panel method with vortex particle wakes," *International Journal for numerical methods in fluids*, Vol. 53, No. 8, 2007, pp. 1399–1422.

³⁶Carrier, J., Greengard, L., and Rokhlin, V., "A fast adaptive multipole algorithm for particle simulations," *SIAM J. Sci. Stat. Comput.*, Vol. 9, No. 4, 1988, pp. 669–686.

³⁷Spalart, P., "Vortex methods for separated flows," *In VKI, Computational Fluid Dynamics, Volume 1 64 p (SEE N89-17818 10-34)*, Vol. 1, 1988.